MnO$_2$ Density - Dependent Supercapacitive Characteristics of SiO$_2$/MnO$_2$ Core-shell Nanostructure

Zhi Qiang Zhang[1,*], Cheng Chen[1], Cong Cong Ma[1], Min Li[2], Hao Chen[1], Zheng Guo Shang[2]

[1]College of Materials Science and Engineering, Chongqing University, Chongqing 400044, PR China
[2]College of Optoelectronic Engineering, Chongqing University, Chongqing 400044, PR China
[*]E-mail: zzqiang1963@163.com

A simple approach has been developed to fine-tune SiO$_2$ spheres into low-density SiO$_2$ spheres with the total volume increased by etching in a NaBH$_4$ solution, followed by the preparation of the SiO$_2$/MnO$_2$ and low-density SiO$_2$/MnO$_2$ core-shell nanocomposites. The core-shell nanocomposites with uniform diameters from 200 to 350nm can be observed on scanning electron microscopy (SEM) and transmission electron microscopy (TEM). With the reaction time increasing, the thickness of manganese oxide shells around the silica core thickens, while the electrochemical properties are observed to present a parabola style. Interestingly, the low-density SiO$_2$/MnO$_2$ core-shell nanocomposites deliver the maximum specific capacitance of 298.3 F g^{-1} far more than the SiO$_2$/MnO$_2$ core-shell nanocomposites (179.8 F g^{-1}), and possess desirable electrochemical stability (5000 cycles retained 86.3%). All of these findings indicate that the low-density SiO$_2$/MnO$_2$ core-shell nanostructures appear to be a promising electrode material for supercapacitors application.

1. INTRODUCTION

Supercapacitors, also known as electrochemical capacitors (ECs), have captured intense attention mostly because of faster and higher power energy storage systems and an exceptional cycle life, filling the gap between batteries and conventional capacitors [1-3]. Generally, ECs can be categorized as electrochemical double layer capacitors (EDLCs) and pseudocapacitors by virtue of the charge storage mechanism [4,5]. The former store energy electrostatically on the basis of charge separation at the electrode/electrolyte interfaces, and pseudocapacitors utilize reversible and rapid superficial Faradaic reactions happening at the electrode. Indeed, electrode materials play an important role in supercapacitors, although various factors can affect the performance of the supercapacitor [6-9]. Among all electrode materials, transition metal oxides (NiO, MnO$_2$, Co$_3$O$_4$, TiO$_2$ and V$_2$O$_5$) are often

preferred, owing to their low internal resistance that contributes to high power output [10-14]. Particularly, as a pseudocapacitive electrode material, MnO_2 manifests outstanding merits on account of its apparent advantages, such as abundance, high theoretical capacity (~1370 F g^{-1}), environmental friendliness and wide potential range in mild electrolyte [15-17].

Recently, there has been extensive interest in the architecture and fabrication of core-shell materials, because of their unique chemical and physical properties and potential applications [18-20]. The coating of shells on cores would alter the charge, functionality and reactivity of the cores and enhance their stability and compatibility, which might provide an available vehicle to obtain hybrid multifunctional materials [21-23]. Silica (SiO_2), easy to form uniform spheres with tunable sizes coated with other materials, is a classic combination which is widely used in many fields [24, 25]. As a matter of fact, silica possess many favorable properties when used in core-shell structures. Firstly, the size of the electro-active materials can be controlled by the sizes of the silica cores. Secondly, the non-agglomerated particles, narrow size distribution and spherical shape offer many sites for the reduction reactions of the electro-active material [26].

Herein, silica via a modified stöber method [25-27] and low-density silica spheres through effective self-templated approach which involves the dissolution of silica cores in a $NaBH_4$ solution and redeposition of the silicate species back onto the colloid surfaces have been synthesized [27]. Using SiO_2 and low-density SiO_2 spheres as templates respectively, we successfully report the synthesis of SiO_2/MnO_2 and low-density SiO_2/MnO_2 core-shell nanocomposites through a facile hydrothermal method. At the same time, the morphology, structure and electrochemical properties of SiO_2/MnO_2 and low-density SiO_2/MnO_2 core-shell nanocomposites are investigated, respectively. Remarkably, the electrode of low-density SiO_2/MnO_2 core-shell nanocomposites demonstrates high supercapacitive performance.

2. EXPERIMENTAL SECTION

2.1 Materials

All the chemical reagents used in the experiments were purchased from Alfa Aesar, which were of analytical purity and used without any further purification.

2.2 Synthesis of SiO₂/MnO₂ core-shell nanocomposites

The uniform silica spheres were synthesized using the modified stöber method. The silica spheres were prepared using ammonia as a catalyst in order to form spherical particles. In a typical synthesis, ethanol (32.5 mL), deionized water (49.5 mL) and ammonia (28 wt. %; 18 mL) were mixed together to form solution A, meanwhile, ethanol (91 mL) and tetraethoxylsilane (2 mL) were mixed to form solution B. After stirring for 10 minutes, B solution was poured into A solution quickly, and then stirred for another 2 h. The mixed starting transparent solution turned into an ivory colloid in the initial

few minutes. To yield a $Si(OH)_2$ gel, the silica colloid was centrifuged and washed with ethanol for several times and then dried at 65 ^{o}C overnight to obtain SiO_2 spheres.

Successively, the silica spheres (0.2 g) were dispersed into the KMnO4 solution (60 mL, 0.05 M) to form a homogeneous precursor. And then, the mixture was poured into a Teflon-lined 100-mL capacity stainless steel autoclave, maintaining at 160 ºC for different reaction time (6 h, 12 h and 24 h, respectively). Finally, the samples were removed, washed with distilled water and ethanol, and dried at 60 ºC to obtain the SiO_2/MnO_2 core-shell nanocomposites.

2.3 Synthesis of low-density SiO_2/MnO_2 core-shell nanocomposites

The silica spheres (0.3 g) and PVP (Polyvinyl Pyrrolidone, 0.25 g) were dispersed into 10 mL deionized water by ultrasonic in a 50-mL beaker. Then $NaBH_4$ powder (0.6 g) was added into the solution. After fully dispersed, the beaker was sealed with sealing membrane and heated in a water bath to maintain at 51 ºC for 6 h to obtain the low-density silica spheres. The resulting products were collected and washed with water and ethanol, finally dried at 65 ºC overnight [27]. The synthesis of low-density SiO_2/MnO_2 core-shell nanocomposites is the same as above.

2.4 Characterization

The crystallographic information of the as-prepared products was established by powder X-ray diffraction (XRD, D/max 2500, Cu Kα) at a scan rate of 0.05º s^{-1} from 5º to 80º. The morphology and structure of the products were carried out with focused ion beam scanning electron microscopy (FIB/SEM, Zeiss Auriga) and transmission electron microscopy (TEM, Zeiss Libra 200).

2.5 Electrochemical measurements

All the electrochemical measurements of nanocomposites synthesized in this work were performed by the electrochemical workstation (CHI 660E) with the electrolyte of 1 M Na_2SO_4 aqueous solution in a three-electrode electrochemical cell. The working electrode was prepared by mixing 70 wt.% active material (SiO_2/MnO_2 and low-density SiO_2/MnO_2 core-shell nanocomposites obtained at different reaction conditions), 20 wt.% acetylene black and 10 wt. % polyvinylidene fluoride (PVDF) in N-methyl-2-pyrrolidone (NMP), and the slurry was spread onto a nickel current collector (1×1 cm^2). The electrode was heated at 120 ºC for 12 h to evaporate the solvent. Platinum plate was used as the counter electrode and saturated calomel electrode (SCE) as the reference electrode. The cyclic voltammetry (CV) and galvanostatic charging/discharging techniques (GCD) which were both tested within a potential window of 1 V were employed to investigate the electrochemical performance of the composites. The applied potential window was ranged from -0.2 V to 0.8 V in a 1 M Na_2SO_4 electrolyte. CVs were recorded as scan rates of 2, 5, 10, 20 and 50 mV s^{-1} and GCD curves were obtained at constant current densities of 0.25, 0.5, 1, 2 and 5 A g^{-1}. The electrochemical impedance

spectroscopy (EIS) was conducted in the frequency range between 100 kHz and 0.01 Hz with a perturbation amplitude of 5 mV versus the open-circuit potential.

3. RESULTS AND DISCUSSION

3.1 Structure and morphology
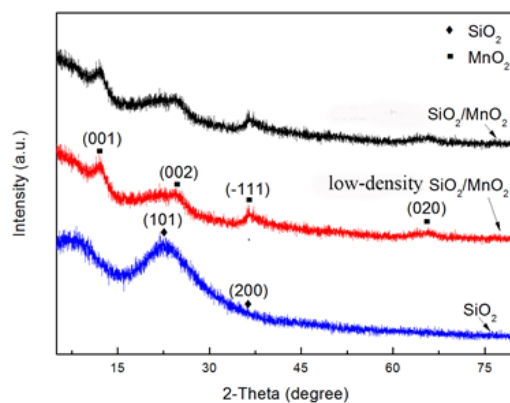
Figure 1. XRD patterns of SiO_2 spheres, SiO_2/MnO_2 and low-density SiO_2/MnO_2 core-shell nanocomposites.
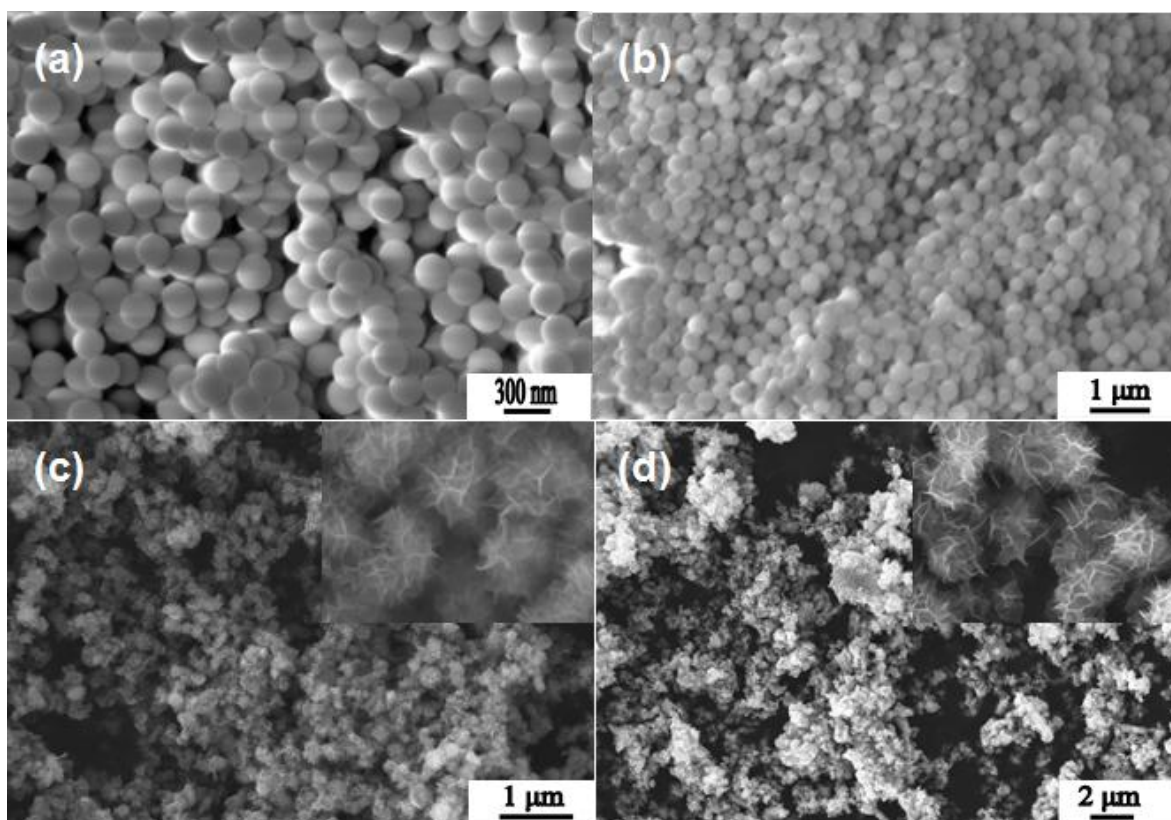
Figure 2. SEM images of (a) SiO_2 spheres; SiO_2/MnO_2 core-shell nanocomposites obtained at 160 ^{o}C (b) 6 h; (c) 12 h; (d) 24 h. The insets of c and d are their higher magnification.

The composition and crystallite phase purity of silica spheres, SiO_2/MnO_2 and low-density SiO_2/MnO_2 core-shell nanocomposites are illustrated in Fig. 1. The as-prepared SiO_2 spheres show a non-crystalline character and there is only one obvious characteristic peak at 21.98° which could be assigned to the (101) planes of the cristobalite SiO_2 (JCPDS file number 39-1425). It can be observed in the XRD pattern of the SiO_2/MnO_2 and low-density SiO_2/MnO_2 core-shell nanocomposites that the diffraction peaks at about 12.5°, 25.2°, 36.6° and 65.6°, assigning to the (001), (002), (-111) and (020) planes respectively, agree well with the standard XRD pattern of birnessite-type manganese oxide crystal (JCPDS 80-1098) [28]. No peaks of impurities can be observed, suggesting the high phase purity of the as-prepared products.

From Fig. 2a we can see that all the SiO_2 spheres enjoy a uniform morphology with diameter of ~250 nm and possess a favorable dispersion in the space. By hydrothermally treating $KMnO_4$ suspension with SiO_2 spheres dispersed at 160 °C for 6 h, 12 h and 24 h, brown intermediate sediment with SiO_2/MnO_2 core-shell nanocomposites were obtained (Fig. 2b-d). Just as depicted in Fig. 2b, there are few MnO_2 nanosheets loaded on the SiO_2 surface after 6 h reaction. However, as the response time extends, SiO_2 spheres are coated with more and more MnO_2 nanosheets, revealing that the SiO_2 spheres could serve as templates to form SiO_2/MnO_2 core-shell nanocomposites very well. The insets of Fig. 2c and d present the detailed morphologies of the as-prepared SiO_2/MnO_2 core-shell nanospheres with intersected nanosheets comprised loosely and distributed homogenously of 12 h reaction and with nanosheets dense packing and bonded together of 24 h reaction time, respectively. Such type of surface morphologies (Fig. 2c) with high specific surface area and pore could greatly enhance the intercalation of the electrolyte ions and ensure sufficient Faradaic reactions [29,30].

After mixing with $NaBH_4$ at the appropriate concentration at 51°C for 6 h, all SiO_2 spheres (250 nm) are converted into well-defined low-density SiO_2 spheres with a diameter of ~200 nm, as shown in Fig. 3a. Although the low-density SiO_2 spheres can be produced without the involvement of any surfactants, PVP is usually added to the reaction system to help prevent interparticle aggregation. Fig. 3b-d exhibit the MnO_2 nanosheets coating on low-density SiO_2 spheres which are reacted at 160 °C for 6 h, 12 h and 24 h to form low-density SiO_2/MnO_2 core-shell nanocomposites. A low-magnification SEM image of these core-shell nanocomposites (Fig. 3) clearly suggests a narrow size distribution. From Fig. 3b-d, one can see that surface of low-density SiO_2 spheres are uniformly covered by close-packed MnO_2 nanosheets and the nanosheets are thicker and thicker with the reaction time increasing due to the Ostwald ripening process. It is worth noting that the diameters of low-density SiO_2/MnO_2 core-shell nanocomposites are changing from 200 nm to 350 nm after loading MnO_2 nanosheets with the increase of reaction time.

The inner structures of low-density SiO_2 spheres, SiO_2/MnO_2 and low-density SiO_2/MnO_2 core-shell nanocomposites are further elucidated by high-resolution TEM (HRTEM, Fig. 4). The uniform and low-density SiO_2 spheres suggest a non-crystalline character which is well consistent with XRD pattern (Fig. 4a, b and Fig. 1). It can be seen in Fig. 4c-e that the surfaces of SiO_2 spheres and low-density SiO_2 spheres are compacted of MnO_2 nanoplates and with lots of pores between MnO_2 nanoplates (Fig. 4c-f). In addition, Fig. 4d and f illustrate the well resolved lattice fringe which gave an interplanar spacing of 0.72 nm and 0.22 nm, consistent with the distance of the (003) planes and (015)

planes of the birnessite-type MnO_2. After reaction with the $NaBH_4$ solution, both the size and density decreased which can increase the specific capacitance of unit mass.
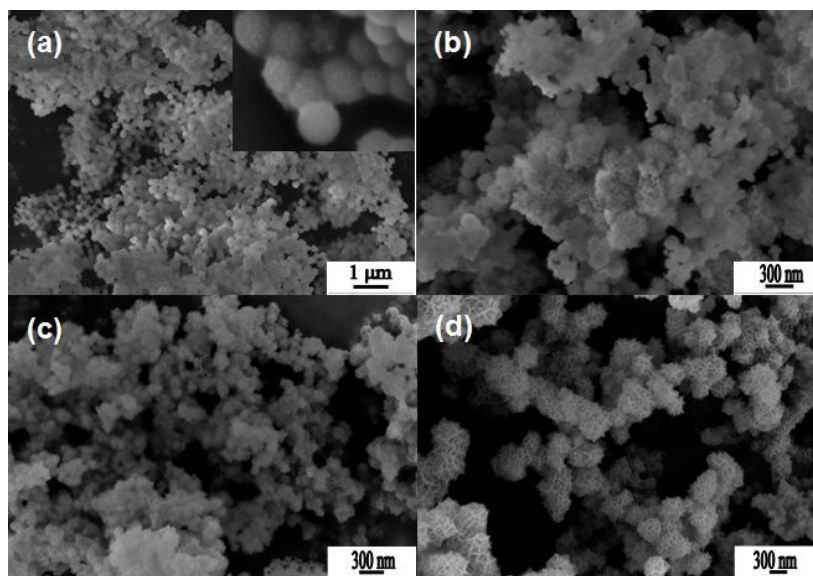
Figure 3. SEM images of (a) low-density SiO_2 spheres; low-density SiO_2/MnO_2 core-shell nanocomposites obtained at 160 °C (b) 6 h; (c) 12 h; (d) 24 h. The inset is the higher magnification.
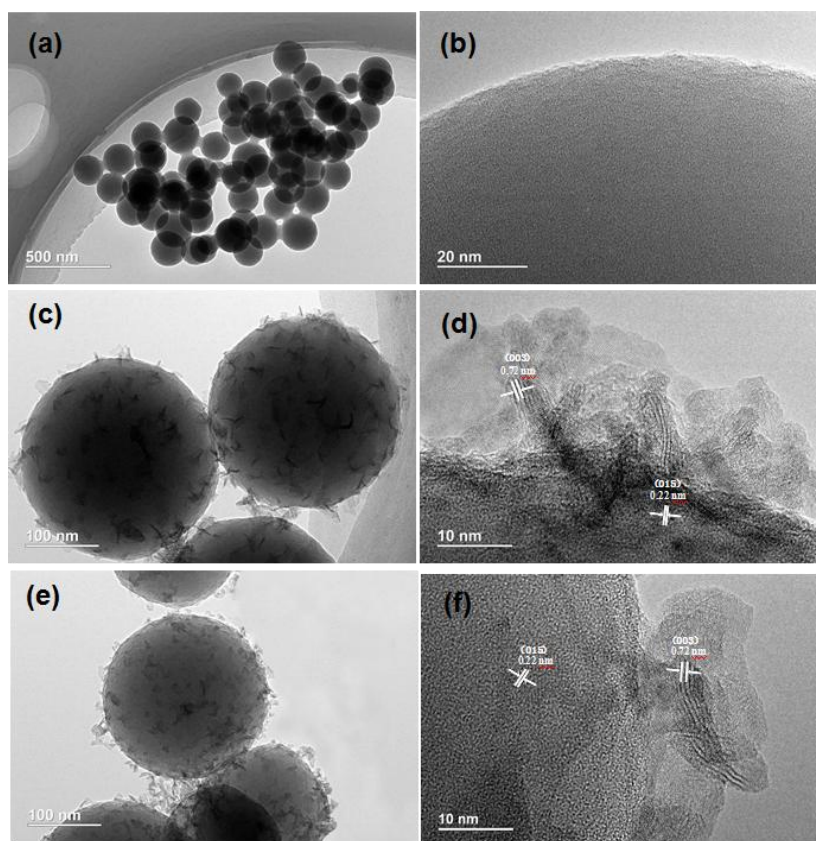
Figure 4. TEM images and HRTEM images of low-density SiO_2 spheres (a, b), SiO_2/MnO_2 (c-d) and low-density SiO_2/MnO_2 core-shell nanostructures (e-f).

3.2 Electrochemical properties

Manganese oxides with various valence states and crystalline structure are currently investigated for electrochemical electronic, catalytic and other applications. Extensive studies have suggested that manganese oxides are promising electrode materials for electrochemical supercapacitors. To evaluate the potential applications in electrochemical capacitors, SiO_2/MnO_2 and low-density SiO_2/MnO_2 core-shell nanocomposites obtained at different reaction time were used to make supercapacitor electrodes in a three-electrode configuration (Fig. 5 and Fig. 6). Cyclic voltammetry is a paramount tool to investigate the capacitive behavior of materials. The CV curves of the SiO_2/MnO_2 and low-density SiO_2/MnO_2 core-shell nanocomposites electrodes with various scan rates ranging from 5 to 50 mV s^{-1} are shown in Fig. 5a and Fig. 6a, which are obtained in a $NaSO_4$ (1 mol L^{-1}) solution. It is clear that the CV curves deviate from the ideal rectangle without distinct redox peaks in the range between -0.2 V and 0.8 V. Notably, from Fig. 5a and Fig. 6a, one can see that the CV curves of the samples obtained at 12 h are larger than that obtained at 6 h and 24 h, manifesting more pleasurable capacitive behavior of the samples obtained at 12 h.
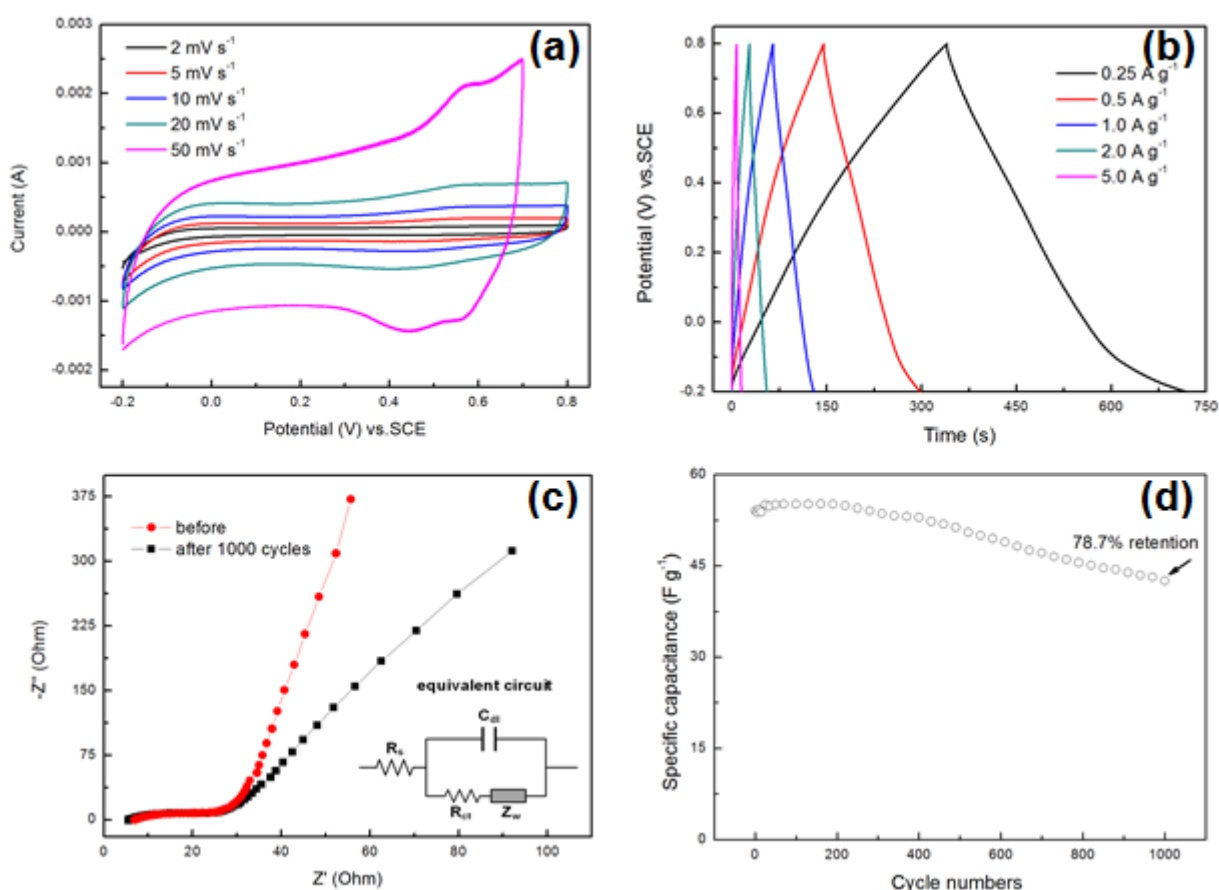
Figure 5. (a) Cyclic voltammograms of SiO_2/MnO_2 core-shell nanocomposites at different scan rate (2, 5, 10, 20 and 50 mV s-1) in a 1 M Na_2SO_4 aqueous electrolyte; (b) charge-discharge curves of SiO_2/MnO_2 core-shell nanocomposites electrodes at different current densities (0.25, 0.5, 1, 2 and 5 A g^{-1}); (c) the electrochemical impedance spectrum of the electrodes at open circuit potential in the frequency range from 0.01 Hz to 100 kHz; (d) cycling performance of SiO_2/MnO_2 core-shell nanocomposites at a current density of 2 A g^{-1}.
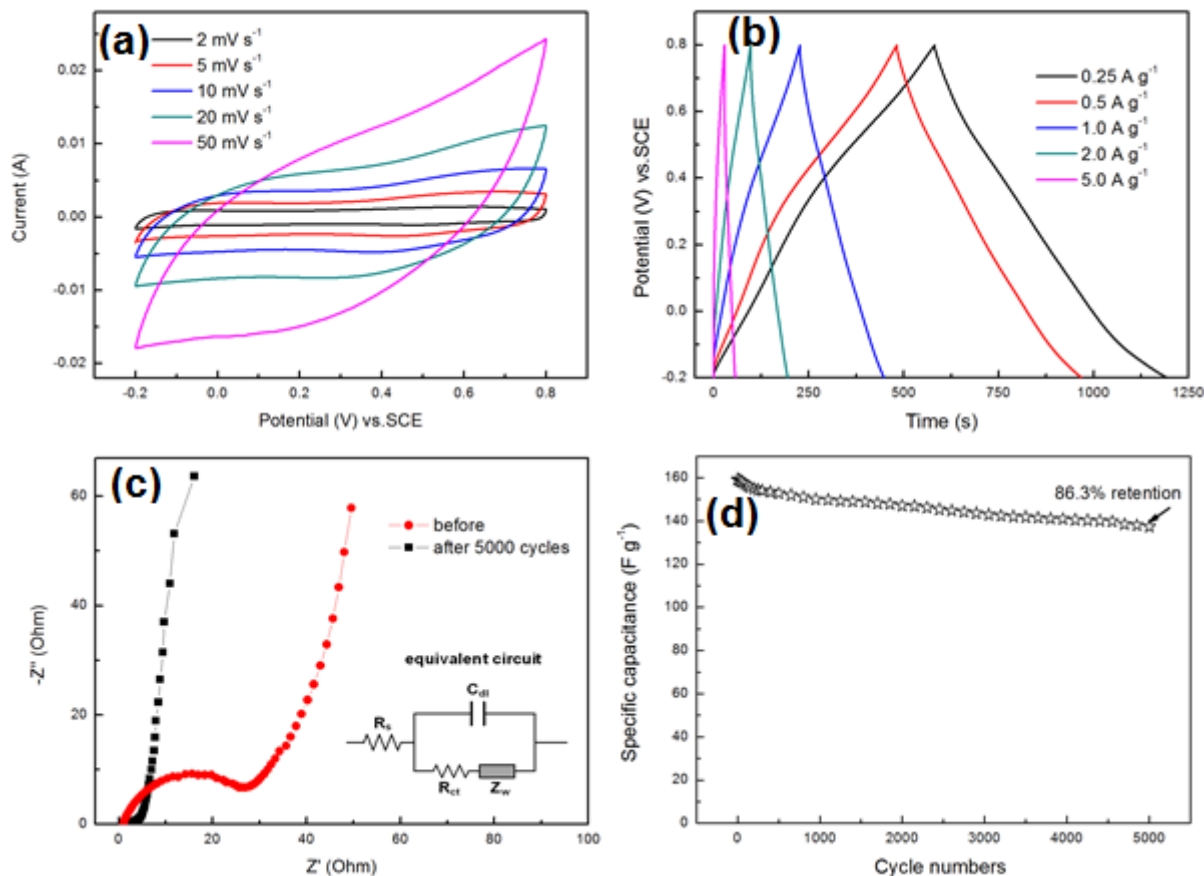
Figure 6. (a) Cyclic voltammograms of low-density SiO_2/MnO_2 core-shell nanocomposites at different scan rate (2, 5, 10, 20 and 50 mV s^{-1}) in a 1 M Na_2SO_4 aqueous electrolyte; (b) charge-discharge curves of low-density SiO_2/MnO_2 core-shell nanocomposites electrodes at different current densities (0.25, 0.5, 1, 2 and 5 A g^{-1}); (c) the electrochemical impedance spectrum of the electrodes at open circuit potential in the frequency range from 0.01 Hz to 100 kHz; (d) cycling performance of low-density SiO_2/MnO_2 core-shell nanocomposites at a current density of 2 A g^{-1}.

Additionally, to further examine the electrochemical performance of the SiO_2/MnO_2 and low-density SiO_2/MnO_2 core-shell nanocomposites electrode, galvanostatic constant current charge-discharge curves (Fig. 5b and Fig. 6b) at various current densities were performed with an electrochemical window of -0.2 to 0.8 V. According to the charge/discharge curves, the specific capacitance (C_m) of electrodes can be calculated according to the following equation:

$$C_m = \frac{I \Delta t}{m \Delta V}$$

Where m, I, Δt and ΔV are the weight (g) of the electroactive materials, discharge current (A), the discharging time (s), and the discharging potential range (V), respectively [31,32]. The specific capacitance values of SiO_2/MnO_2 and low-density SiO_2/MnO_2 core-shell nanocomposites obtained at 12 h calculated from galvanostatic constant current charge-discharge curves are found to be 179.8 F g-1 and 298.3 F g^{-1}, respectively. After tuning the silica spheres to low-density silica sphere, the specific of low-density SiO_2/MnO_2 core-shell nanocomposites is 1.7 times larger than SiO_2/MnO_2 core-shell nanocomposites, which may attribute to the larger specific surface area under the same quality.

The remarkable electrochemical characteristic is attributed to the nanostructured electrode materials, which generates a high electrode/electrolyte contact area and short path lengths for electronic transport and electrolyte ion. While, it is clearly that both the SiO_2/MnO_2 and low-density SiO_2/MnO_2 core-shell nanocomposites made at 12 h (Fig. 5b and Fig. 6b) have longer charge-discharge time than the samples prepared at 6 h and 24 h, respectively. We also compared the specific capacitance with the similar results from previously reported publications (Table 1). Low density SiO_2/MnO_2 displayed superior electrochemical performance may be due to the several aspects: (i) based on the mechanism of pseudocapacitance, ion intercalation is one of reaction during charging and/or discharging for MnO_2. Thus, the path of ion transportation does not need long enough. i.e., long path will be difficult for ions to accelerate moving in and moving out. Herein, we tune the loading and density of MnO_2 nanosheets to investigate the optimal ion intercalation effect for pseudocapacitance. (ii) $NaBH_4$ was used to reduce few of silica to silicon and increase the conductivity of composites without removing SiO_2 core. (iii) the present findings have proved that the low-density SiO_2/MnO_2 core-shell nanocomposites deliver the maximum specific capacitance of 298.3 F g^{-1} far more than the SiO_2/MnO_2 core-shell nanocomposites (179.8 F g^{-1}), and have desirable electrochemical stability (5000 cycles retained 86.3%).

Table 1. Comparison with the other reported results.

Samples	Electrolyte	Test condition	Cs (F g^{-1})	References
SiO_2/MnO_2	0.1 M Na_2SO_4	0.2 A g^{-1}	197	33
$SiC@SiO_2$ nanocables/MnO_2	1 M Na_2SO_4	0.2 A g^{-1}	276.3	34
SiC/B-MnOx	1 M Na_2SO_4	10 mV s^{-1}	251.3	35
MnO_2/HGC nanosphere	1 M Na_2SO_4	5 mV s^{-1}	380	36
MnO_2/HPCs-75	1 M Na_2SO_4	20 mV s^{-1}	417.2	37
Porous MnO_2	1 M Na_2SO_4	2 mV s^{-1}	205	38
porous ZrO_2-SiO_2	2 M KCl	1 A g^{-1}	312.6	39
Co_3O_4/SiO_2	5 M KOH	2.5 mV s^{-1}	758	40
Co_3O_4/SiO_2	5 M KOH	2.5 mV s^{-1}	1143	41
SiO_2	1 M Et_4NBF_4/PC	100 mA g-1	62.5	42
MnO_2/3D-G	1 M Na_2SO_4	0.5 A g^{-1}	310.0	43
MnO_2 hollow spheres	0.5 M Na_2SO_4	2 mV s^{-1}	159.2	44
low-density SiO_2/MnO_2	1 M Na_2SO_4	0.25 A g^{-1}	298.3	This work

As depicted in Fig. 5c and Fig. 6c, the impedance plots were measured in the frequency range of 0.01-100 kHz at open circuit potential by applying an AC voltage with 5 mV amplitude of SiO_2/MnO_2 and low-density SiO_2/MnO_2 core-shell nanocomposites electrode before and after 1000 cycles and 5000 cycles, respectively. It can be obviously seen that both of their impedance spectra were almost similar in form, consisted of one semicircle at the high frequency and followed by a linear part at the low-frequency. As we can see, the inset of Fig. 5c displays the equivalent circuit for the Nyquist plots. It is universally acknowledged that electrochemical stability is one of the key properties that the supercapacitor devices need to have. And Fig. 5d and Fig. 6d show the long-term cycling performance of SiO_2/MnO_2 and low-density SiO_2/MnO_2 core-shell nanocomposites by galvanostatic charge-discharge process at the current density of 2 A g^{-1} for practical applications for consecutive 1000 cycles and 5000 cycles, respectively. SiO_2/MnO_2 core-shell nanocomposites shows a retention of 78.7 % after 1000 cycles which indicated the SiO_2/MnO_2 core-shell structure do not have good cycling

stability, while low-density SiO_2/MnO_2 core-shell nanocomposites shows a retention of 86.3 % after 5000 cycles which suggested the moderate stability toward long time charge–discharge applications and further confirming the excellent supercapacitive and superior electrochemical reversibility, indicating that the controllable synthesis of low-density SiO_2/MnO_2 core-shell nanocomposites structure is a promising material for electrochemical capacitors application.

4. CONCLUSIONS

In summary, a flexible, cost-effective and green approach has been established to manufacture SiO_2/MnO_2 and low density SiO_2/MnO_2 core-shell nanocomposites. Compared with the specific capacitance of SiO_2/MnO_2 core-shell nanocomposites (179.8 F g^{-1}), the low density SiO_2/MnO_2 core-shell nanocomposites deliver higher capacitance of 298.3 F g^{-1}. The SiO_2/MnO_2 and low density SiO_2/MnO_2 core-shell nanocomposites show retention of 78.7 % after 1000 cycles, and 86.3 % after 5000 cycles, respectively, indicating a desirable electrochemical stability. These findings indicate that the low density SiO_2/MnO_2 core-shell nanocomposites could be a promising and cost-effective active material in electrochemical stable supercapacitors for practical application.

References

1. P. Simon, Y. Gogotsi, *Nat. Mater.*, 7 (2008) 845.
2. L. Dimesso, S. Jacke, C. Spanheimer, W. Jaegermann, *J. Alloys Compd.*, 509 (2011) 3777.
3. M. Winter, R.J. Brodd, *Chem. Rev.*, 104 (2005) 4245.
4. R.R. Salunkhe, K. Jang, H. Yu, S. Yu, T. Ganesh, *J. Alloys Compd.*, 509 (2011) 6677.
5. Q.T. Qu, L. Li, S. Tian, W.L. Guo, Y.P. Wu, *J. Power Sources*, 195 (2010) 2789.
6. J.X. Zhu, W.H. Shi, N. Xiao, X.H. Rui, Q.Y. Yan, *ACS Appl. Mater. Interfaces*, 4 (2012) 2769.
7. M. Huang, Y.X. Zhang, F. Li, Q. Liu, *Sci. Reports*, 4 (2014) 4518.
8. Z.X. Song, W. Liu, M. Zhao, Y.J. Zhang, J.S. Qiu, *J. Alloys Compd.*, 560 (2013) 151.
9. Z.Q. Zhang, C.C. Ma, M. Huang, F. Li, Y.X. Zhang, *J. Mater. Sci: Mater. Electron.*, 6 (2015) 4212.
10. S.Q. Ci, Z.H. Wen, Y.Y. Qian, J.H. Chen, *Sci. Reports*, 119 (2015) 19.
11. L. Li, R.M. Li, S.L. Gai, Y.J. Chen, P.P. Yang, *J. Mater. Chem.* A, 3 (2015) 15641.
12. M. Lee, S.K. Balasingam, H.Y. Jeong, Y. Jun, *Sci. Reports*, 5 (2015) 8151.
13. C. Feng, J.F. Zhang, Y. He, C. Zhong, W.B. Hu, L. Liu, Y.D. Deng, *ACS Nano*, 9 (2015) 1730.
14. C.C. Zhang, C.J. Peng, B. Gao, X. Peng, X.M. Zhang, J.J. Fu, *J. Nanomater.*, 2015 (2015) 7.
15. X.J. Ma, W.B. Zhang, L.B. Kong, Y.C. Luo, L. Kang, *New. J. Chem.*, 39 (2015) 6207.
16. C. Choi, S.H. Kim, H.J. Sim, J.A. Lee, A.Y. Choi, Y.T. Kim, S.J. Kim, *Sci. Reports*, 5 (2015) 9387.
17. L. Li, Z.A. Hu, N. An, Y.Y. Yang, Z.M. Li, H.Y. Wu, *J. Phys. Chem.*, 118 (2014) 22865.
18. F. Caruso, Adv. Mater., 12 (2001) 11.
19. V. Skumryev, S. Stoyanov, Y. Zhang, G. Hadjipanayis, D. Givord, J. Nogues, *Nature*, 423 (2003) 850.

20. A.L. Yarin, E. Zussman, J.H. Wendorff, A. Greiner, *J. Mater. Chem*., 17 (2007) 2585.
21. X.D. Su, J.Z. Zhao, X. Zhao, Z.C. Wang, *Nanotechnology*, 19 (2008) 365610.
22. Z.Q. Zhang, C.C. Ma, L. He, M. Huang, L. Yu, Y.X. Zhang, *Ceram. Int*., 40 (2014) 10309.
23. J. Yu, H.Y. Chen, M.H. Chen, N. Liu, Q.W. Li, *ACS Appl. Mater. Interfaces*, 5 (2013) 3408.
24. S.H. Ryu, S.G. Hwang, S.R. Yun, K.K. Cho, K.W. Kim, K.S. Ryu, *Bull. Korean. Chem. Soc*., 32 (2011) 2683.
25. G.A.M. Ali, O.A. Fouad, S.A. Makhlouf, M.M. Yusoff, K.F Chong, *Adv. Engineering*, 18 (2014) 2505.
26. G. Lia, Z. Wanga, M. Yua, Z. Quana, J. Lin, *J. Solid. State. Chem*., 179 (2006) 2698.
27. T. Zhang, Q. Zhang, J.P. Ge, J. Goebl, M.W. Sun, Y.S. Yan, Y.S. Liu, C.L. Chang, Y.D. Yin, *J. Phys. Chem*. C, 113 (2009) 3168.
28. Y.X. Zhang, M. Huang, F. Li, X.L. Wang, Z.Q. Wang, *J. Power Sources*, 246 (2014) 449.
29. S. Peng. L. Li, H. Tan, S. Ramakrishna, M. Srinivasan, Q. Yan, *J. Mater. Chem*. A, 1 (2013) 7630.
30. Y.X. Zhang, M. Kuang, J.J. Wang, *CrystEngComm.,* 16 (2014) 492.
31. Y. Cheng, H. Zhang, S. Lu, C.V. Varanasi, J. Liu, *Nanoscale*, 5 (2013) 1067.
32. J. Li, H, Xie, *Mater. Lett*., 78 (2012) 106.
33. S. Ryu, S. Hwang, S. Yun, K. Cho, K. Kim, K. Ryu, *Chem. Soc*., 8 (2011) 2683.
34. Y. Zhang, J. Chen, H. Fan, K. Chou, X. Hou, *Dalton Trans.***,** 44 (2015) 19974.
35. M. Kim, J. Kim, ACS Appl. Mater. Interfaces, 6 (2014) 9036.
36 J. Lv, X. Yang, H. Zhou, L. Kang, Z. Lei, Z. Liu, *Materials Research Bulletin*, 73 (2016) 429.
37. H. Li, L. Jiang, Q. Cheng, Y. He, V. Pavlinek, P. Saha, C. Li, Electrochimica Acta, 164 (2015) 252.
38. C. Wan, L.Yuan, H. Shen, *Int. J. Electrochem. Sci.,* 9 (2014) 4024.
39. G. H. Jeong, H. Lee, J. Kang, H. Lee, C. Kim, J. Lee, J. Kim, S. Kim, *ACS Appl. Mater. Interfaces*, 6 (2014) 20171.
40. G. A. M. Ali, O. A. Fouad, S. A. Makhlouf, M. M. Yusoff,   K. F. Chong , *Adv. Mat. Res*., 1133 (2016) 447.
41. Gomaa A. M. Ali , Osama A. Fouad, Salah A. Makhlouf, Mashitah M. Yusoff, *J. Solid. State. Electrochem.*, 18 (2014) 2505.
42. X. Du, C. Wang, T. Li, M. Chen, *Ionics*, 15 (2009) 561.
43. S. Sun, P. Wang, S. Wang, Q. Wu, S. Fang, *Mater. Lett*., 145 (2015) 141.
44. H. Z. Chi, S. Yin, H. Qin, K. Su, *Mater. Lett*., 162 (2016) 131.